Color-Contrast of Single Layer Graphene under White Light Illumination Induced by Broad-band Photon Management

Xiaobai Yu,[1,#] Sidan Fu[1,#], Yi Song,[2,] Haozhe Wang,[2] Xiaoxin Wang[1], Jing Kong[2,*], Jifeng Liu[1,*]

[1] Thayer school of Engineering, Dartmouth College, 14 Engineering Drive, Hanover, New Hampshire 03755, USA

[2] Department of Electrical Engineering and Computer Science, Massachusetts Institute of Technology, 77 Massachusetts Avenue, Cambridge, Massachusetts 02139, USA

# X.Y. and S.F. contributed equally to this work.

*Corresponding authors, email addresses:

Jifeng.Liu@dartmouth.edu (J.F.)

JingKong@mit.edu (J.K.)

ORCID:

Xiaobai Yu: 0000-0001-9228-6584

Sidan Fu: 0000-0002-5391-8056

Haozhe Wang: 0000-0001-5123-1077

Jing Kong: 0000-0003-0551-1208

Jifeng Liu: 0000-0003-4379-2928

Abstract:

Visualizing and manipulating the optical contrast of single layer graphene (SLG) and other 2D materials has continuously been an interesting topic to understand fundamental light-matter interaction down to atomic thickness. Since the optical properties of SLG can be tuned by gating, demonstrating and manipulating the color contrast of SLG also has significant potential applications in ultra-thin flexible color display. However, previous demonstrations of optical contrast of SLG are mostly limited to reflection intensity contrast under monochromatic illumination using interference effect. The reported spectral contrast in SLG has mostly been narrow-band or at resonant wavelengths, and it required precise thickness control and/or nanolithography that are hardly scalable to large enough area for display applications. In this paper, we demonstrate novel color-contrast optical visibility of SLG under white light using broad-band photon management induced by nanoneedle structured SnO_x ($x \leq 1$) transparent conductive oxides (TCOs), which is scalable to large-area color display. The low-temperature fabricated, self-assembled, nanoneedle structured SnO_x ($x \leq 1$) thin films help to significantly increase the *broadband* optical absorption in SLG by enhancing the electromagnetic field and increasing the scattering efficiency at the SnO_x/SLG interface. With nanoneedle structured SnO_x, the optical absorption in SLG on fused quartz (SiO_2) substrate is drastically increased from ~1.4% to >10 % at λ=560-990 nm (from yellow to near infrared spectral regimes), leading to a clear color contrast to the surrounding region without SLG. The self-assembly approach, rather than sophisticated and costly nanolithography, allows scalable fabrication of large area 2D photonic devices with broadband and highly efficient photon management effect. Therefore, this approach

can be further extended to color-tunable TCO/dielectric/SLG 2D photonic devices by adjusting the free carrier concentrations/Fermi levels in the TCO and SLG layers via gating - a stepping stone towards ultra-thin flexible color display technologies utilizing 2D materials and nanostructured thin films.

Keywords: Photon management, single layer graphene, color contrast, SnO_x nanoneedle, transparent conducting oxide (TCO), 2D photonics

Introduction

Among various kinds of two dimensional (2D) materials, single layer graphene (SLG) has drawn enormous interest. Due to its atomic thickness and the unique conical band structures, the electronic and mechanical properties of SLG have been widely investigated for flexible devices and transparent electrodes in solar cell applications.[1, 2] Optically, free standing SLG is perceived as nearly transparent since it only absorbs 2.3 % of the incident light, independent of wavelength.[3] This number goes down to 1.4 % if SLG is transferred on fused quartz (SiO_2) substrate due to optical impedance mismatch.[4] Therefore, optically visualizing SLG has been a challenging topic to understand fundamental light-matter interactions down to atomic thickness.

Novoselov et al.[5], for the first time, found SLG was visible on top of a thermal oxidized Si wafer using the interference effect from 300 nm-thick SiO_2. Geim et al.[6] subsequently noted that precise control of the oxide thickness is required to visualize SLG, and a 5 % thickness variation can make SLG invisible. Blake et al.[7] studied the visibility of SLG more systematically. They demonstrated the dependence of the SLG visibility on SiO_2 thickness and incident wavelength, and corroborated the observations by a model based on Fresnel Law. With this established concept, later researchers experimented with a variety of thicknesses and other materials, including Si_3N_4 and SiO_2/Si_3N_4 bilayers to visually identify the number of graphene layers,[8, 9] a PMMA layer to enhance the visibility of SLG on various substrates,[10] and various dielectric films (SiO_2, $BaTiO_3$, HfO_2, Al_2O_3, Si_3N_4, $SrTiO_3$) to investigate their influences on the contrast of mono- and bilayer graphene.[11]

However, these existing techniques rely on the interference effect by precisely engineering the optical paths in materials, which is highly dependent on optimizing the wavelength of the incident light and the thickness and refractive index of the dielectric layer(s). That is, the region with SLG shows the same color but typically darker than the region without SLG under the optimal illumination wavelength. For example, Khadir et al.[12] and Li et al.[13] utilized interferometry to enhance the SLG intensity contrast at specific wavelengths of 625 nm and 532 nm. Blake et al.[7], Jung et al.[9], Kontis et al.[11], and Chen et al.[14] demonstrated narrow-band or resonant wavelengths enhancements by precise control of the dielectric layer thicknesses. Therefore, most of the previous reports demonstrated *intensity* contrast under optimal monochromatic illumination instead of *color* contrast under white light illumination, where the regions with and without SLG would show different colors.

Besides utilizing photonic layer stacks to visualize graphene monochromatically, understanding and enhancing the light-matter interaction for 2D absorbers has continuously been a very active field of study. Very recent progress demonstrated a graphene-dielectric-metal heterostructure where enhanced graphene absorption is achieved through far-field excitation of plasmon modes squeezed into an atomically thin dielectric spacer between graphene and metal nanostructures. [15] Similarly, other people reported plasmonically enhanced graphene photo-detectors with high responsivity and fast speed. [16] These approaches, though, not only require sophisticated and costly nanolithography, but also work only for a narrow band of mid- or far-infrared wavelengths. Therefore, they are not compatible with large-area consumer devices such as flexible flat panel display, which

requires broadband photon management for color contrast visibility. There has barely been any research on this significant potential application of 2D materials and photonic devices.

In this paper, we demonstrate color-contrast optical visibility of SLG under white light using broad-band photon management induced by self-assembled nanoneedle-structured SnO_x ($x \leq 1$) transparent conductive oxides (TCOs). The near-field interaction between the SnO_x TCO and SLG leads to a strongly enhanced broad-band absorption in SLG from the visible to the near infrared (NIR) spectral regime, as confirmed by strong field-enhanced Raman scattering from SLG, thereby inducing a clear color contrast between the regions with and without SLG. Since the self-assembly of nanostructured SnO_x TCO can be readily scaled to large-area fabrication, just like their counterparts currently used in flat panel display, this approach can be extended to color-tunable TCO/dielectric/SLG 2D photonic devices by adjusting the free carrier concentrations/Fermi levels in the TCO and SLG layers, enabling new flexible color display technologies utilizing 2D materials and nanostructured thin films. This vision is further supported by recent progress in growing large-area graphene >20 inches in dimensions. [17]

TCO thin films are widely used in flat panel display technology. Combined with active absorber layers, they are also widely used for light-trapping in optoelectronic devices.[18, 19, 20, 21, 22, 23, 24, 25] Thanks to their broad-band transparency, effective photon management ability and high electrical conductivity, TCO is more advantageous than conventional light trapping strategies such as plasmonics and dielectric nanostructures. [26, 27] By comparison, metallic (Au or Ag) plasmonic structure is cost-intensive and has a narrow resonant peak, while dielectric nanostructures are insulating and the fabrication is

complicated. Surface textured TCO has been proved to be an effective tool for light trapping in thin film solar cells, but the relatively large surface roughness (~100 nm) [28, 29] impairs the light trapping effect on thinner (<1 μm thickness) absorbers and limits its application in 2D photonic devices. Therefore, we propose a nanoneedle-structured Sn-rich SnO (SnO_x, x<1) TCO thin film with surface roughness <5 nm to couple with SLG. As demonstrated in our previous work, [30, 31, 32] these nanoneedle-structured SnO_x (x<1) thin films can be fabricated by co-sputtering Sn and SnO_2 at adequate ratios, followed by low-temperature thermal annealing at 200-250°C. Details of the fabrication process is provided in the Methods section. Due to the greatly reduced surface roughness, light scattering is not significantly dependent on the surface texturing but on the inherent nanoneedle structures. This low-temperature self-assembly approach significantly reduces the cost compared to conventional patterning and sophisticated nanolithography, which allows scalable fabrication of large area devices for displays. In our previous research [31, 32], a SnO_x (x~0.85) nanoneedle-structured TCO thin film has been proved to be very effective in enhancing the efficiency of thin film Ge NIR photodetectors, contributing to a 10-30× enhancement of photocurrent with a scattering efficiency >95 % for light trapping in Ge. In this study, we further extend this SnO_x nanoneedle-structured TCO thin film to light trapping in 2D SLG and demonstrate color-contrast visibility of SLG under white light illumination, pushing the envelope of photon management as the active absorber thickness decreases to atomic scale. Notably, it has not yet been reported that TCOs could be used for light trapping in active 2D absorbers. Therefore, our innovative approach of combining SLG with low temperature-fabricated, high scattering-efficiency nanostructured TCOs

opens up new paths to understand high-efficiency light trapping and extend the application of TCO photon management to practical 2D photonic devices.

Results and Discussion

Optical Contrast of SLG.

Figure 1a shows a schematic drawing of nanoneedle-structured SnO_x($x \leq 1$)/SLG/quartz with the light illuminating from the SnO_x side. An atomic force microscopy (AFM) image is shown in the inset. Owing to the field enhancement in the vicinity of the high refractive index Sn-rich regions [4] and high scattering efficiency of the self-assembled SnO_x nanoneedle structures, [31, 32] the effective light trapping in SnO_x/SLG/quartz leads to a strong color contrast of SLG under white light illumination that is visible to the naked eye, as illustrated in **Figure 1b**. As a reference, the area of SLG/quartz is nearly transparent with no perceivable difference from the quartz substrate alone (see the region labelled as "SLG" in Fig. 1b). Notably, adding a layer of 115 nm SnO_x ($x \sim 0.85$) on top of SLG results in a strong color contrast between the central area with SLG (bluish, labelled as "SnO_x+SLG") and the peripheral edge without SLG (pinkish, labelled as "SnO_x"). The SnO_x/SLG/quartz region appears bluish compared to the surrounding pinkish SnO_x/quartz region because longer wavelength light from yellow to red regime is much more effectively absorbed by SLG due to the photon management in this region, as will be detailed later. Hence, the color of the SnO_x/SLG/quartz region is more influenced by shorter wavelength photons under white light illumination, leading to a bluish appearance compared to the pinkish peripheral region without SLG.

For the same piece of sample with transferred SLG in the middle, the optical absorption contrast contributed by SLG is calculated as the difference in absorption between the regions with and without SLG. As shown in **Figures 1c and 1d**, the maximum optical absorption enhancement in SLG reaches ~15% at λ=670-770 nm due to the photon management of the 115 nm-thick, nanoneedle-structured SnO_x layer, representing >10× absorption enhancement compared to pristine graphene on silica (~1.4% [4]). Because of the p-type doping effect of pristine SLG transferred to the quartz substrate, the absorption diminishes at longer wavelengths corresponding to the blue curve in **Figure 1d** at λ>1500 nm. In contrast, the light trapping effect induced by nanoneedle structured SnO_x happens over a broad-band spectral regime (i.e. SLG absorption=4-15% over λ=400-2000 nm according to **Figure 1d**), thanks to the n-type compensation doping effect introduced by the Sn nanostructures [4] in SnO_x (as revealed by the diffraction peaks of β-Sn in **Figure 2g**). Such a highly effective and broad-band light trapping effect leads to a strong color contrast between the regions with and without SLG under white light illumination, which is a notable improvement in visualizing SLG compared to the conventional interference-induced intensity contrast under optimal monochromatic illumination. Our previous work [4] reported self-assembled, pseudo-periodic ultrahigh refractive index Sn nanodots for SLG absorption enhancement in the NIR regime. However, it only demonstrated absorption intensity contrast instead of color contrast in the visible regime. While reducing the nominal thickness of Sn nanodots could better match the SLG absorption enhancement with the visible spectrum, it also induces a much larger morphological difference between the Sn nanostructures deposited on SLG vs. those deposited on quartz [4] that overwhelms the color contrast induced by photon management. By comparison, in this paper the optical

color contrast is achieved in the visible spectrum regime, and it is predominantly contributed by the SLG absorption enhancement without any morphological differences between the SnO_x nanostructures deposited on SLG vs. those on quartz. This will be detailed in the next section.

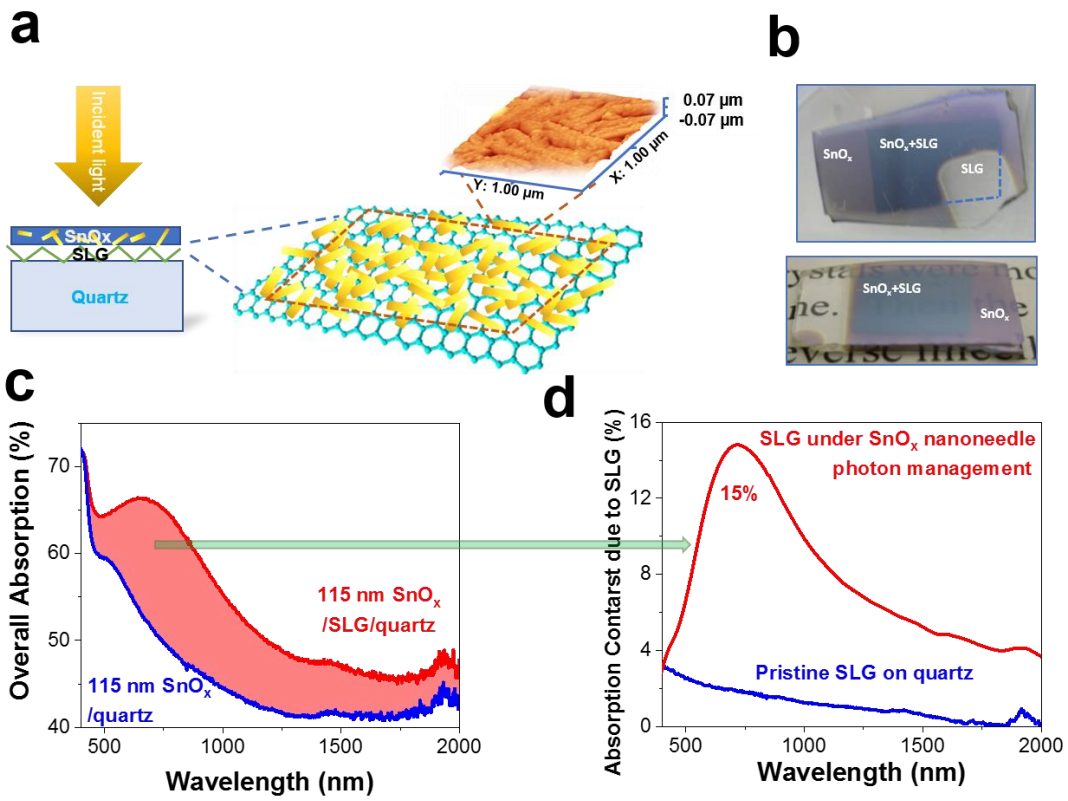

Figure 1 (a) A schematic drawing of the SnO_x/SLG/quartz structure. A typical atomic force microscopy image of the structure is also shown on top of the schematic drawing. **(b)** Photographs of 115 nm-thick nanoneedle-structured SnO_x/SLG/quartz (x~0.85) samples. Color contrast of SnO_x/SLG (bluish) can be clearly observed compared to SLG on quartz (transparent) or SnO_x on quartz (pinkish) alone. These photographs demonstrate light-trapping induced optical visibility of SLG under white light illumination. **(c)** Overall absorption spectra of the SnO_x/SLG/quartz sample (red curve) and the reference SnO_x/quartz sample (blue curve). The red shaded area corresponds to the absorption contributed by SLG in the SnO_x/SLG/quartz region, as presented by the red line in (d). **(d)** The absorption contrast spectra contributed by SLG in the SnO_x/SLG/quartz samples (red curve) in comparison to that of the pristine SLG/quartz sample (blue curve). The absorption contrast due to SLG refers to the absorption difference between the area with SLG and the surrounding area without SLG on the same sample. A maximal absorption contrast of 15% contributed by SLG in the SnO_x/SLG/quartz samples is observed at λ=670-770 nm,

representing >10× absorption enhancement compared to the reference SLG on quartz (~1.4% absorption).[4]

Morphology and Microstructure of Nanoneedle-Structured SnO_x on SLG.

To exclude any morphological variation in the SnO_x nanoneedles on SLG compared to that on the surrounding area without SLG, nanoneedle-structured SnO_x grown on SLG/quartz was characterized by scanning electron microscopy (SEM) and atomic force microscopy (AFM). We found that the morphology of the self-assembled SnO_x nanoneedles grown on SLG/quartz (**Figure 2b**) still resembles that of the SnO_x directly deposited on quartz (**Figure 2a**), i.e. the SLG underneath has no observable impact on the growth of the SnO_x nanoneedle nanostructure. Therefore, these results confirm that the absorption contrast between the regions with and without SLG shown in **Figure 1** is not due to the corresponding morphological differences in SnO_x nanostructures. As will be shown later, the optical contrast is predominantly due to the enhanced absorption in SLG via photon management of nanoneedle-structured SnO_x, as confirmed by Raman peak intensity analyses of Sn, SnO, and SLG. At a higher magnification (**Figure 2c**), granular structures on each nanoneedle can be clearly observed. Figure S3 further reveals the detail of the granular topography in AFM. The average root-mean-square roughness R_{rms} is <5 nm and the average peak-to-peak roughness R_{pp} is <8 nm, much smaller than the wavelength of interests and the typical surface roughness induced by the conventional TCO surface textures (on the order of 100 nm).

In addition, the front side (i.e. the surface) and the back side (i.e. the interface in contact with SLG) of the SnO_x thin film show differences in secondary electron (SE) and back scattered electron (BSE) modes. Brighter parts in the BSE mode correspond to Sn-rich regions since the atomic number of Sn is higher than O. In **Figure 2c**, the front side of

the thin film in the SE mode clearly consists of densely packed SnO_x nanoneedles with a few interspersed Sn nanostructures. At the same area, the BSE mode (**Figure 2d**) reveals some bright Sn-rich regions within or near each needle, which makes it look like a Sn-SnO core-shell structure. As supported by the X-ray diffraction (XRD) spectrum in **Figure 2g**, the only existing crystalline phases in SnO_x were tetragonal SnO (ICDD 00-006-0395) and β-Sn (ICDD 00-004-0673). A different perception can be obtained by looking at the backside of the thin film grown on SLG, i.e. the interface in contact with SLG. This interface was exposed by using a piece of conductive tape to peel the SnO_x thin film off the SLG layer on the quartz substrate. Raman spectroscopy (**Figure 3d**) has verified that the SLG remained on quartz and still maintained its structure from before peeling SnO_x. Since SnO_x was deposited on a relatively flat 2D layer of SLG, the backside surface is fairly smooth, which makes a better BSE contrast with minimal perturbation from the surface roughness. Due to the flatness of this backside interface, the outline of the nanoneedles are barely seen in SE mode (**Figure 2e**), yet it shows clear contrast of the Sn cores/network and contours of nanoneedles from BSE imaging (**Figure 2f**). The darker nanoneedle body is a bit narrower than the original estimate based on the SE morphology alone. The average width is estimated to be around 80 nm. Although the Sn distribution is fairly complicated, to the first order approximation, optically these structures can still be modelled as Sn/SnO core-shell nanoneedles with random orientations.

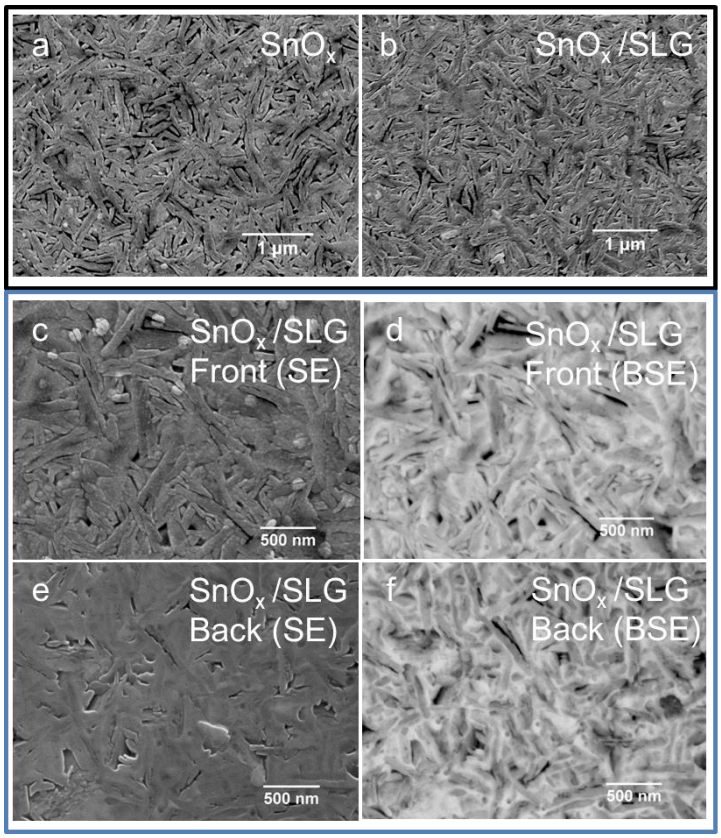

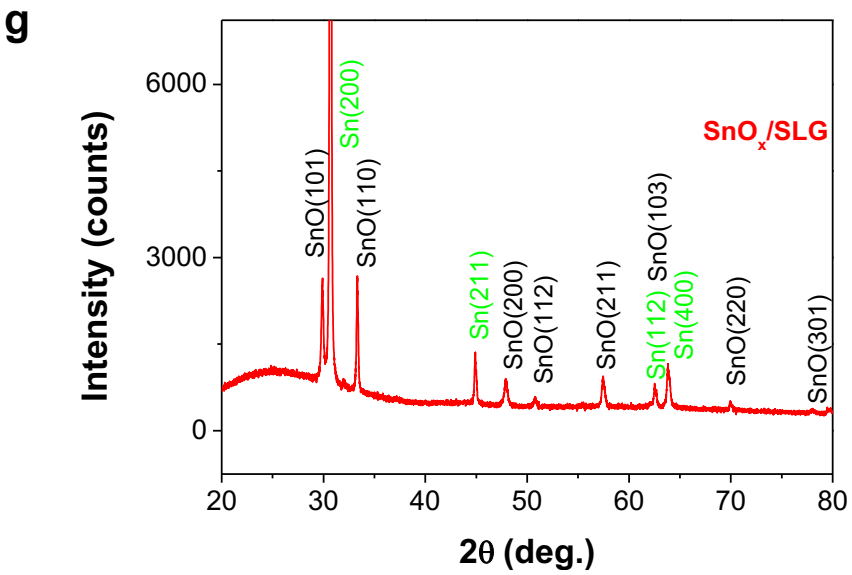

Figure 2 SEM images of **(a)** SnO_x/quartz (x=0.85) and **(b)** SnO_x/SLG/quartz (x=0.85) regions on the same sample, showing no observable difference in morphology and microstructure; **(c)** and **(d)** show the front side of SnO_x on SLG/quartz in SE and BSE modes, respectively; **(e)** and **(f)** show the back side of SnO_x (i.e. the interface in contact with SLG) in SE and BSE modes, respectively, suggesting a Sn/SnO core-shell nanoneedle

structure. **(g)** XRD data of the SnO_x/SLG/quartz sample. The nanoneedle thin film consists of tetragonal SnO (ICDD 00-006-0395) and β-Sn (ICDD 00-004-0673) crystal phases after crystallization annealing in N_2 at 225 °C for 20 min.

Field Enhanced Raman Scattering from SLG in SnO_x Nanoneedles/SLG Regions.

Raman spectroscopy analyses are performed to examine the quality of SLG upon co-sputtering of Sn and SnO_2 and verify the SLG absorption enhancement attributed to the SnO_x nanoneedle photon management. **Figure 3 a-c** show the Raman spectra of the pristine SLG/quartz (i.e. blue lines) and 115 nm $SnO_{0.85}$/SLG/quartz samples (i.e. red lines) under the excitation wavelengths of 532 nm, 633 nm, and 785 nm respectively. While the pristine SLG/quartz shows clear G bands (~1600 cm^{-1}) and 2D bands (~2600 cm^{-1}) which are both intrinsic Raman signals from defect-free graphene, the 115 nm SnO_x/SLG/quartz presents significant D bands (~1350 cm^{-1}). The D band, as an indicator of lattice disorder in graphene [33, 34], suggests that the sputtering or annealing process of SnO_x on SLG induces a deviation from the perfect 2D hexagonal lattice. Figure S4 further compares the Raman spectra of the SnO_x/SLG/quartz sample before and after the thermal annealing process to form the nanoneedle structure, as mentioned earlier in the introduction and detailed in Methods section. Clearly, the D band is already quite strong even before the thermal annealing. This result indicates that the origin of the D band in SnO_x/SLG/quartz samples is the sputtering process rather than the annealing process.

Figure 3d further demonstrates the Raman spectra of a 145 nm-thick $SnO_{0.85}$/SLG/quartz sample (red curve) and the same area after peeling off the SnO_x layer (blue curve), at an excitation wavelength of 514 nm. Obviously, removing the SnO_x layer does not recover SLG from the lattice disorder, suggesting an irreversible modification in the 2D lattice from the sputtering process. The phenomenon that the energetic sputtered

atoms (10-100 eV) can impair the C-C symmetric lattice of graphene has been reported in the past. [35,36,37] In this case, the D-band is mostly induced by atomic-scale surface undulations (≤1Å) of the 2D layer after interacting with energetic Ar ions [35]. On the other hand, as confirmed in Figure S5, such an atomic-scale surface undulation has very little impact on the optical absorption in SLG at λ =500 – 900 nm, corresponding to the wavelength range of photon management effect. We will also discuss how to prevent such sputtering-induced lattice disorder in SLG in the later text.

Moreover, Raman peak intensity enhancement [4] can be used to further confirm the enhanced optical absorption in SLG under photon management. The Raman scattering intensity is approximately proportional to $|E|^4$ [38] while the optical absorption is proportional to $|E|^2$ [39], where E is the electric field of the optical excitation wave. Hence, a stronger Raman peak intensity directly indicates a field enhancement and an enhanced optical absorption. Quantitatively, for SLG, this phenomenon can be described as [4]

$$\frac{I_{D+G+2D}(SLG\ under\ SnOx)}{I_{D+G+2D}(SLG)} / F_{Lattice-Disorder} \approx \frac{|E|^4}{|E_0|^4} \cdot T_{Raman} \quad (1)$$

Here, $I_{D+G+2D}(SLG\ under\ SnO_x)$ and $I_{D+G+2D}(SLG)$ refer to the integrated Raman peak intensities of SLG with and without SnO_x nanoneedle photon management, respectively (i.e. the blue shaded and red shaded areas in **Figure 3a-d,** respectively); E and E_0 are the electric fields in SLG with and without SnO_x nanoneedle photon management respectively. Considering that the Raman-scattered photons generated in the SLG region must transmit through any layer on top of the SLG (i.e. SnO_x nanoneedle in this case) in order to be collected by the Raman spectroscopy system, a term T_{Raman} is multiplied to represent the transmittance of the Raman-scattered photons. While the transmittance of Raman-scattered photons is close to 100% for the SLG/quartz reference sample, it is

dramatically reduced in 115 nm SnO_x/SLG/quartz samples due to the enhanced absorption of SLG (refer to **Figure 1c**) and the scattering/absorption of the SnO_x nanoneedles. Considering that the transmittance loss of the quartz substrate is negligibly small, T_{Raman} can be well approximated by the experimentally measured transmittance of the 115 nm SnO_x/SLG/quartz sample at the Raman scattering wavelengths, as listed in **Table 1** and further detailed in Figure S6. Moreover, a term $F_{Lattice\text{-}Disorder}$ is also divided, representing the change in the integrated Raman peak intensity due to the atomic-scale surface undulation of the SLG lattice introduced by the energetic sputtering process. This factor is calculated by comparing the SLG integrated Raman peak intensity of the 145 nm SnO_x/SLG/quartz sample *after peeling off* SnO_x (i.e. the blue line in Fig. 3d) to that of pristine SLG/quartz sample under the same excitation condition. As detailed in Figure S7, this factor is determined to be 0.90, very close to 1. Such a result is also consistent with the optical data in Figure S5, showing that the lattice disorder induces little change in the optical absorption of SLG at λ=500-900 nm. Therefore, we can derive the field enhancement $|E|^2/|E_0|^2$ from the Raman spectroscopy data using Eq. 1, which would also be equal to the absorption enhancement in SLG theoretically. As shown **Table 1**, the relative field enhancements $|E|^2/|E_0|^2$ derived from Raman spectroscopy and the transmittance of the Sn/SLG/ quartz sample at excitation wavelengths of λ = 532, 633, and 785 nm are in good agreement with the absorption enhancement measured in **Figure 1c** (within 10% relative error range). For the 145 nm-thick SnO_x/SLG/quartz and 174 nm-thick SnO_x/SLG/quartz samples, the same analyses have been performed as shown in Figure S8-S9 and Table S1-S2. All these results support the highly effective photon

management and optical absorption enhancement in SLG by utilizing self-assembled SnO_x nanoneedle structures, leading to the optical color contrast shown in **Figure 1b**.

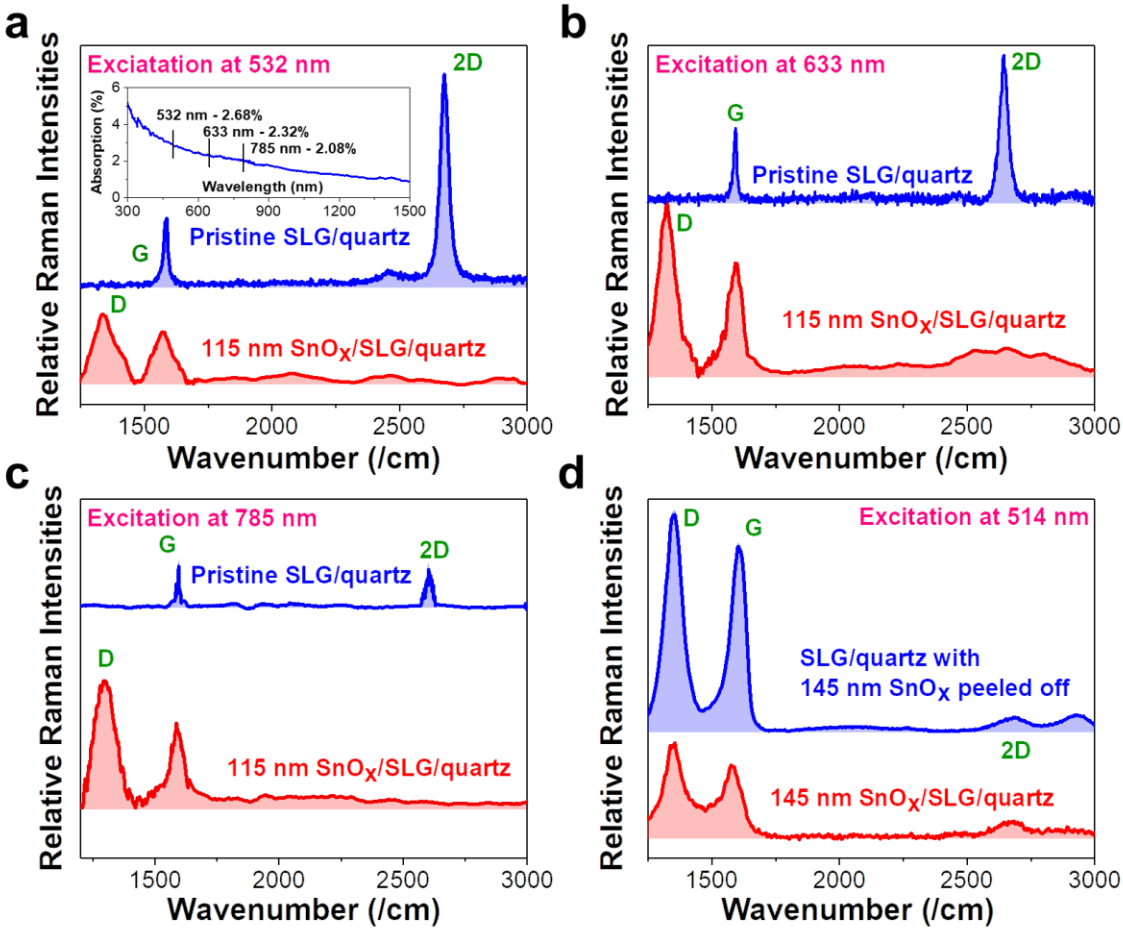

Figure 3 Raman spectra of pristine SLG/quartz samples (blue lines) and 115 nm $SnO_{0.85}$/SLG/quartz samples (red lines) at excitation wavelengths of **(a)** 532 nm; **(b)** 633 nm; and **(c)** 785 nm, respectively. The inset of (a) corresponds to the optical absorption spectrum of the pristine SLG/quartz sample, which will be used in the quantitative analysis in **Table 1**. **(d)** is a comparison of the Raman spectra of 145 nm $SnO_{0.85}$/SLG/quartz sample before vs. after peeling off the SnO_x layer at an excitation wavelength of 514 nm. The blue and red shaded areas correspond to the integrated Raman peak intensities that will be used in the quantitative analysis in **Tables 1, S1 and S2**. The Raman spectra at the excitation wavelengths of 532 nm, 633 nm, and 785 nm are measured by a different Raman system than that of 514 nm, which leads to the difference in signal-noise level from (a-c) to (d).

Raman spectra of SnO and β-Sn in SnO_x nanostructures have also been analyzed to verify that the color contrast is predominantly due to the enhanced SLG absorption. SnO

is known to have Raman peaks at 110 cm^{-1} and 210 cm^{-1}. [40] As shown in Figure S10 and Table S3, it is clear that the absorption of SnO has not been modified between SnO_x/SLG/quartz and SnO_x/quartz. Similarly, β-Sn is known to have a Raman peak at 125 cm^{-1}. [41] From Figure S10, again, there is no evidence of any significant change in the β-Sn Raman band (appearing as a shoulder at ~125 cm^{-1} in the spectra). These further confirm that the absorption of Sn and SnO is similar or identical between SnO_x/SLG/quartz and SnO_x/quartz, supporting our conclusion that the optical color contrast shown in **Figure 1b** is predominantly due to enhanced SLG absorption.

Table 1 Summary of Raman intensity ratios of I_{D+G+2D} (SLG under SnO_x)/ I_{D+G+2D} (SLG) at different excitation wavelengths, the corresponding transmittance of Raman-scattered photons through the SnO_x/SLG nanostructures (T_{Raman}), the estimated SLG field enhancement $|E|^2/|E_0|^2$ in SLG from Eq. 1, the SLG absorption derived from Raman scattering enhancement (i.e. $SLG\ field\ enhancement * pristine\ SLG\ absorption$), and the SLG absorption measured by UV-VIS-IR spectrometer from **Figure 1c**, based on 115 nm SnO_x/SLG/quartz sample under the excitation wavelengths of 532 nm, 633 nm, and 785 nm respectively.

Excitation Wavelength	Measured Integrated SLG Raman Peak Intensity Ratio $\frac{I_{D+G+2D}(SLG\ under\ SnOx)}{I_{D+G+2D}(SLG)}$	Transmittance of Raman-Scattered Photons T_{Raman}	SLG Field Enhancement $\frac{E^2(SLG\ under\ SnOx)}{E^2(SLG)}$	SLG Absorption Derived from Raman Enhancement (%)	SLG Absorption from UV-Vis-IR spectroscopy in Figure 1c (%)
532 nm	0.938	0.265	1.982	5.31	5.77
633 nm	4.677	0.308	4.107	9.53	10.46
785 nm	13.238	0.310	6.888	14.33	14.77

To further explore the mechanism of SLG photon management effect and investigate an approach to avoid the lattice disorder of SLG upon sputtering, we deposit a very thin layer of GeO_2 (i.e. 10 nm and 20 nm) on SLG by thermal evaporation before sputtering the SnO_x layer. Such a thin layer of GeO_2 is transparent under visible and near infrared (NIR) light. According to **Figure 4a**, the optimal SLG absorption does drop significantly as the

thickness of GeO_2 layer increases, indicating that the optical interaction between SnO_x nanoneedles and SLG is essentially a near field effect. On the other hand, the evaporated GeO_2 layer protects the SLG lattice from disorder upon sputtering, as shown by the Raman spectra in **Figure 4b**. The thermal evaporation of GeO_2 itself did not introduce any lattice damage to SLG. This is because atoms from the thermal evaporation are much less energetic (~0.1 eV) [42] than from the sputtering (10-100 eV). In other words, GeO_2 film functions as a protective layer for the SLG lattice. For the 10 nm GeO_2, although the peak absorption of SLG is somewhat reduced compared to the case without GeO_2 (10.5% vs. 15%), it still achieves 7-8× absorption enhancement compared to the reference SLG/quartz sample (1-2% according to **Figure 1c**). Such an enhanced SLG absorption has also been confirmed by quantitative analysis of the integrated Raman peak intensities in **Figure 4b** and **Table 2**. Furthermore, the GeO_2 insulator layer offers the capability to gate SLG by applying a voltage between SnO_x and SLG, thereby tuning the absorption of the SnO_x/GeO_2/SLG for tunable photon management. Therefore, this approach provides a great potential for future application in 2D photonic devices.

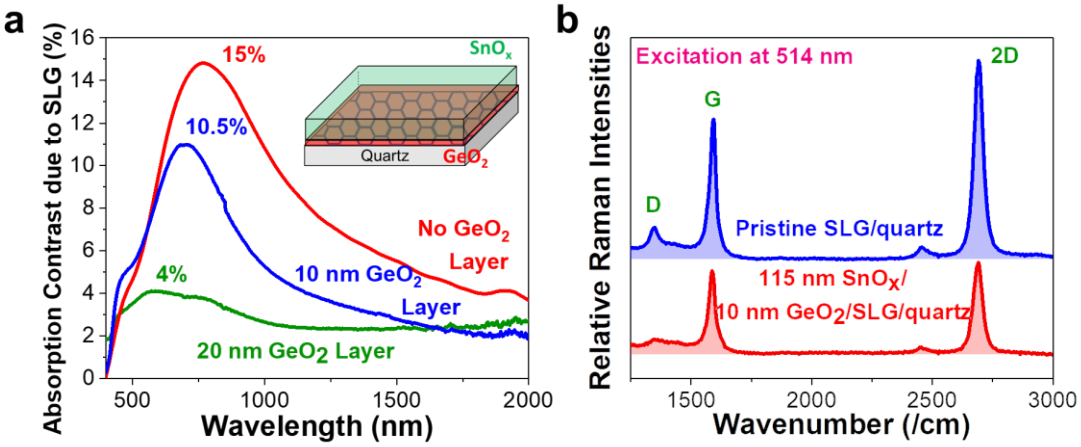

Figure 4 (a) SLG absorption contrast spectra of 115 nm-thick SnO_x/GeO_2/SLG/quartz samples with different thicknesses of GeO_2, i.e. 0 nm (red line), 10 nm (blue line), and 20 nm (green line). The optimal SLG absorption decreases with the thickness of GeO_2 layer, indicating that the photon management in SLG is mainly contributed by the near-field optical interactions between SnO_x and SLG. (b) Raman spectra of pristine SLG/quartz sample (blue line) in comparison with 115 nm SnO_x/10 nm GeO_2/SLG/quartz sample (red lines), under the excitation of 514 nm. Quantitative analysis of the integrated Raman peak intensities can be found in **Table 2**.

Table 2 Summary of Raman intensity ratios of I_{D+G+2D} (SLG under SnO_x)/ I_{D+G+2D} (SLG) at different excitation wavelengths, the corresponding transmittance of Raman-scattered photons through the Sn/SLG nanostructures (T_{Raman}), the estimated SLG field enhancement $|E|^2/|E_0|^2$ in SLG from Eq. 1, the SLG absorption derived from Raman scattering enhancement (i.e. $SLG\ field\ enhancement * pristine\ SLG\ absorption$), and the SLG absorption measured by UV-VIS-IR spectrometer from **Figure 1c**, based on 115 nm SnO_x/10 nm GeO_2/SLG/quartz sample under the excitation wavelengths of 514 nm.

Excitation Wavelength	Measured SLG Raman Field Intensity Ratio $\frac{I_{D+G+2D}(SLG\ under\ SnOx)}{I_{D+G+2D}(SLG)}$	Transmittance of Raman-Scattered Photons T_{Raman}	SLG Field Enhancement $\frac{E^2(SLG\ under\ SnOx)}{E^2(SLG)}$	SLG Absorption derived from Raman enhancement (%)	SLG Absorption Measured by UV-VIS-IR spectroscopy (%)
514 nm	0.811	0.229	1.987	5.36	5.65

As discussed earlier (**Figure 2g**), the SnO_x layer contains Sn and SnO phases. Sn, a group IV semimetal that is compatible with Si for applications in practical semiconductor devices, possesses a much higher refractive index [43] over the NIR light regime. This allows a much stronger near-field enhancement at nanoscale (i.e. > 100× optical field intensity at the airgap between Sn nanostructures) and thereby a much higher absorption enhancement of SLG in the vicinity of Sn nanodots, as we have reported elsewhere. [4] A similar mechanism can be expected in the SnO_x nanoneedle-based photon management strategy here considering that we have indeed observed Sn/SnO core-shell nanoneedles from the BSE images in Figures 2d and 2f. The near-field enhancement of Sn nanostructures is also consistent with the observation that the SLG absorption enhancement decreases

dramatically with the GeO_2 thickness in Figure 4a, which defines the minimal spacing between Sn nanoneedles and SLG. Furthermore, we have verified the importance of excess Sn composition (compared to stoichiometric SnO) to the photon management effect by controlling the value x in SnO_x, as illustrated in Figure S11. Clearly, strong SLG absorption enhancement only occurs in Sn-rich SnO. Moreover, the nanoneedle structure itself effectively enhances the scattering efficiency of the incident light, [31, 32] and consequently contribute to the broad-band absorption enhancement of SLG absorption for better optical color contrast.

Conclusion

In conclusion, we demonstrate a novel SLG photon management strategy that utilizes a self-assembled, low-temperature fabricated, nanoneedle-structured SnO_x TCO thin film. By coating SnO_x nanoneedles on the top, the absolute optical absorption of SLG can be effectively enhanced up to ~15% over visible and near infrared light regimes - a significant improvement compared to 1-2% absorption in the pristine SLG material. The broad-band photon management leads to a clear color contrast between the regions with and without SLG and makes the atomically thin layer SLG clearly visible under white light illumination with naked eyes. This color-contrast optical visibility of SLG stands out from the existing strategies that only reveals the optical contrast of SLG in a narrow spectral regime under optimal monochromatic illumination using the interference effect of precisely thickness-controlled dielectric layers. Such an enhanced absorption in SLG has also been confirmed by strongly enhanced integrated Raman peak intensities. The low-temperature self-assembly approach allows for scalable large-area fabrication for 2D photonic devices.

In addition, we also provide an approach to protect the integrity of the 2D SLG hexagonal lattice while maintaining most of the photon management effect by introducing an ultrathin GeO_2 layer between SnO_x and SLG. Moreover, it can be foreseen that via electrical gating, [44, 45, 46] the SnO_x (conductor)/GeO_2 (insulator)/SLG structure will achieve tunable color contrast, potentially enabling SLG-based ultra-thin flexible color display that has barely been envisioned or investigated before. These results suggest a promising way to utilize nanostructured SnO_x TCOs for broadband, tunable photon management in 2D materials towards novel flexible color display technologies.

Methods

Preparation of Single Layer Graphene.

Single layer graphene (SLG) was synthesized via chemical vapor deposition (CVD) [47] on a 25 μm-thick Cu foil (99.8% purity, Alfa Aesar) and then transferred to fused quartz substrates via a layer of polymethyl methacrylate (PMMA) [48]. To prepare the substrate for CVD, the Cu foil was soaked in nickel etchant (Transense, TFB) for 90 s and rinsed with deionized water. It was then heated in a CVD chamber at 1030 °C exposed to a mix of 3.5 sccm CH_4 and 60 sccm H_2 for 30 min. After the synthesis of the SLG, a 1:1 dilution of PMMA (950 A9, Microchem Inc.) and anisole was spin-coated on it at 2500 rpm for 1 min, followed by an 80°C annealing for 1 h. Copper etchant (Transense, TFB) was then used to remove the Cu foil. After etched with 10% HCl for 10 min and rinsed with deionized water, the PMMA/SLG was freed from the Ni and was ready to be transferred to the fused quartz substrate. Subsequently, PMMA/SLG/quartz was baked at 80 °C for 8 h and 130 °C for 20 min. Then, the stack was soaked in acetone at room temperature for 1 h, followed by a

second annealing at 350 °C with a mix of 200 sccm H_2 and 200 sccm Ar for 2 h to remove the PMMA.

Preparation of Self-assembled SnO_x Thin Films.

SnO_x nanoneedle-structured thin films of 115 nm, 145 nm and 175 nm thicknesses were fabricated via a non-reactive co-sputtering process by a Lab 18 PVD machine (Kurt J. Lesker). The co-sputtering of Sn and SnO_2 took place in an Ar environment (Ar pressure=2.7×10^{-3} Torr). The base vacuum was better than 5×10^{-8} Torr before deposition. The deposition rates of Sn and SnO_2 were determined in an earlier research [30] to ensure the reproducibility of the chemical composition and stoichiometry for optical property optimization. The elemental composition was analyzed and the stoichiometric formula (x=0.85) was determined by Rutherford backscattering spectroscopy (RBS). [30]

In this experiment, we used nominal sputtering rates of Sn and SnO_2 at 1.1 Å/s and 0.2 Å/s monitored by a quartz crystal oscillator to get a non-stoichiometric amorphous SnO_x (x<1). The crystallization and self-assembling of Sn and SnO occurred during a subsequent tube furnace (Thermolyne F21100) annealing at 225 °C for 20 min in a N_2 atmosphere. During annealing, Sn and SnO_2 self-assembled to form crystalline SnO, nanoneedles.[30] Simultaneously, some of the excess Sn crystallized and segregated, interspersing among the SnO nanoneedles. As will be discussed later, it can be optically described as a Sn/SnO core/shell nanoneedle structure. As discussed in Ref. [30], the annealing temperature (close to the melting temperature of Sn) and the annealing ambient are significant to obtaining the structure, which helps to reduce surface segregated Sn, maintaining the function of Sn as scatterer inside the film.

Preparation of GeO_2 Thin Films.

The GeO_2 dielectric/protective layers was thermally evaporated onto SLG by a Lab18 Physical Vapor Deposition (PVD) system produced by Kurt J. Lesker Company. The chamber was pumped to a based vacuum of 5×10^{-8} Torr. The evaporation source material, GeO_2, was provided by Kurt J. Lesker company with 99.99% purity. The substrate was kept rotating at 20 rounds per minute during the entire evaporation process to avoid non-uniformity in the thin film growth. The substrate temperatures were controlled at ~25 °C by chilled water. The typical deposition rate of GeO_2, read by the quartz crystal monitor during deposition, was ~0.1 Å/sec.

Morphological and Raman Characterization.

A FEI XL-30 scanning electron microscope (SEM) and a Vecco Dimension 3100 atomic force microscope were employed in this research to compare the morphology and the surface topography of the SnO_x/quartz and SnO_x/SLG/quartz films. SEM was also used for characterizing the thickness of a cross-sectional SnO_x thin film made by this deposition recipe. (See Figure S1 in the Supporting Information) This thickness was determined earlier in this research to demonstrate an optimal visual contrast in SLG. However, to prove the less dependency of the SLG visibility on the film thickness compared to those highly thickness-dependent interference-dominant dielectric films, thicknesses up to 174 nm have been tested and verified as well for showing an optical enhancement and color contrast in SLG. (See Figure S2 in the Supporting Information) The change in vibrational modes and Raman enhancements in SLG at the excitation wavelength of 514 nm were characterized by a Witec Confocal Raman system; that at the excitation wavelengths of 532 nm, 633 nm, 785 nm were characterized by a Horiba LabRAM Raman system. The crystalline phases

in the thin films were confirmed by a Rigaku DMax rotating anode X-ray diffraction (XRD) system with Cu kα radiation (λ=1.54 Å).

Optical Characterization.

A Jasco V-570 spectrometer with an integrating sphere was employed to acquire transmittance and reflectance spectra from λ = 300 to 2500 nm. The absorption is calculated by

Absorption = 1 - Transmittance - Reflectance (2a).

As discussed later, the morphology of SnO_x on SLG remained identical to that of SnO_x on quartz. Thereby, we can calculate the absorption contrast due to SLG (i.e. absorption difference by comparing the area with SLG and the surrounding area on the same sample) by subtracting the absorption of SnO_x/quartz from that of SnO_x/SLG/quartz, that is,

Absorption (SLG) = Absorption (SnO_x/SLG/quartz) – Absorption (SnO_x/quartz) (2b)

Associated Content

Supporting Information

The Supporting Information is available free of charge on ACS Publications websites at DOI:

Cross-Sectional SEM of SnO_x thin film, SLG enhanced absorption spectra varying thickness, SnO_x thin film surface AFM, Raman spectra of SnO_x/SLG/quartz before/after annealing, Absorption spectra of sputtering-modified SLG/quartz vs. pristine SLG/quartz, Transmittance spectra of SnO_x/SLG/quartz samples varying SnO_x thicknesses, Raman

spectra of sputtering-modified SLG/quartz vs. pristine SLG/quartz, Raman analysis of SLG absorption under 145 and174 nm-thick SnO_x photon management, Raman analyses of SnO and β-Sn absorption, and Dependence of photon management effect in SLG on the stoichiometry of SnO_x nanoneedles.

Funding Sources

This work has been sponsored by National Science Foundation under the collaborative research Awards #1509272 and #1509197.

Acknowledgement

We greatly appreciate the help from the Electron Microscope Facility at Dartmouth College. We would also like to thank Dr. Christopher Levey for helpful discussions.

Notes

The authors declare no competing financial interest.

References

(1) Novoselov, K. S.; Geim, A. K.; Morozov, S. V.; Jiang, Zhang, D. Y.; Dubonos, S. V.; Grigorieva, I. V.; Firsov, A. A. Electric Field Effect in Atomically Thin Carbon Films. *Science* **2014**, 306 (5696), 666-669.

(2) Widjaja, H.; Jiang, Z.; Altarawneh, M.; Yin, C.; Goh, B.; Mondinos, N.; Amri, Amun; Dlugogorski, B. Z. Double-sided F and Cl Adsorptions on Graphene at Various Atomic

Ratios: Geometric, Orientation and Electronic Structure Aspects. *Appl. Surf. Sci.* **2016**, 373, 65-72.

(3) Nair, R. R.; Blake, P.; Grigorenko, A. N.; Novoselov, K. S.; Booth, T. J.; Stauber, T.; Peres, N. M. R.; Geim, A. K. Fine Structure Constant Defines Visual Transparency of Graphene. *Science* **2008**, 320 (5881), 1308–1308.

(4) Fu, S.; Wang, H.; Wang, X.; Song, Y.; Kong, J.; Liu, J. Self-Assembled, Ultrahigh Refractive Index Pseudo-Periodic Sn Nanostructures for Broad-Band Infrared Photon Management in Single Layer Graphene. *ACS Photonics* **2019**, 6 (1), 50-58.

(5) Novoselov, K. S.; Jiang, D.; Schedin, F.; Booth, T. J.; Khotkevich, V. V.; Morozov, S. V.; Geim, A. K. Two-Dimensional Atomic Crystals. *PNAS* **2005**, 102 (30) 10451-10453.

(6) Geim, A. K.; Novoselov, K. S. The Rise of Graphene. *Nat. Mater*. **2017**, 6, 183-191.

(7) Blake, P.; Hill, E. W. Making Graphene Visible. *Appl. Phys. Lett.* **2017**, 91, 063124.

(8) Ni, Z. H.; Wang, H. M.; Kasim, J.; Fan, H. M.; Yu, T.; Wu, Y. H.; Feng, Y. P.; Shen, Z. X. Graphene Thickness Determination Using Reflection and Contrast Spectroscopy, *Nano Lett*. **2007**, 7 (9), 2758-2763.

(9) Jung, I.; Rhyee, J.; Son, J. Y.; Ruoff, R. S.; Rhee, K. Colors of Graphene and Graphene-Oxide Multilayers on Various Substrates. *Nanotechnology*, 2012, 23 (2), 025708.

(10) Teo, G.; Wang, H.; Wu, Y.; Guo, Z.; Zhang, J.; Ni, Z.; Shen, Z. Visibility Study of Graphene Multilayer Structures. *J. Appl. Phys.* **2008**, 103, 124302.

(11) Kontis, C.; Mueller, M. R.; Kuechenmeister, C.; Kallis, K. T.; Knoch, J. Optimizing the Identification of Mono- and Bilayer Graphene on Multilayer Substrates. *Appl. Opt*. **2012**, 51(3), 385-389.

(12) Khadir, S.; Bon, P.; Vignaud, D.; Galopin, E.; McEvoy, N.; McCloskey, D.; Monneret, S.; Baffou, G. Optical Imaging and Characterization of Graphene and Other 2D Materials Using Quantitative Phase Microscopy. *ACS Photonics* **2017**, 4, 3130−3139.

(13) Li, W.; Moon, S.; Wojcik, M.; Xu, K. Direct Optical Visualization of Graphene and Its Nanoscale Defects on Transparent Substrates. *Nano Lett.* **2016**, 16, 5027−5031.

(14) Chen, T.; Mastropaolo, E.; Bunting, A.; Stevenson, T.; Cheung, R. Optimization of the Visibility of Graphene on Poly-Si Film by Thin-Film Optics Engineering. *J. Vac. Sci. Technol B* **2012**, 30, 06FJ01.

(15) Iranzo, D. A.; Nanot, S.; Dias, E. J. C.; Epstein, I.; Peng, C.; Efetov, D. K.; Lundeberg, M. B.; Parret, R.; Osmond, J.; Hong, J.; Kong, J.; Englund, D. R.; Peres, N. M. R.; Koppens, F. H. L. Probing the ultimate plasmon confinement limits with a van der Waals heterostructure. *Science* **2018**, 360, 291-295.

(16) Ma, P.; Salamin, Y.; Baeuerle, B.; Josten, A.; Heni, W.; Emboras, A.; Leuthold J. Plasmonically Enhanced Graphene Photodetector Featuring 100 Gbit/s Data Reception, High Responsivity, and Compact Size. *ACS Photonics* **2019**, 6, 154-161.

(17) Chen, X.; Chen, Z.; Jiang, W.; Zhang, C.; Sun, J.; Wang, H.; Xin, W.; Lin, L.; Priydarshi, M. K.; Yang, H.; Liu, Z.; Tian, J.; Zhang, Y.; Zhang, Y.; Liu, Z. Fast Growth and Broad Applications of 25-Inch Uniform Graphene Glass. *Adv. Mater.* **2017**, 29, 1603428, 1-9.

(18) Tak, Y.; Kim, K.; Park, H.; Lee, K.; Lee, J. Criteria for ITO (Indium–Tin-Oxide) Thin Film as the Bottom Electrode of an Organic Light Emitting Diode. *Thin Solid Films* **2002**, 411, 12–16.

(19) Chae, G. S. A Modified Transparent Conducting Oxide for Flat Panel Displays Only.

Jpn. J. Appl. Phys. **2001**, 40 (3R), 1282.

(20) Shah, A. V.; Schade, H.; Vanecek, M.; Meier, J.; Vallat-Sauvain, E.; Wyrsch, N.; Kroll, U.; Droz, C.; Bailat, J. Thin-Film Silicon Solar Cell Technology. *Prog. Photovolt. Res. Appl.* **2004**, 12, 113–142.

(21) Dagkaldiran, ü.; Gordijn, A.; Finger, F.; Yates, H. M.; Evans, P.; Sheel, D. W.; Remes, Z.; Vanecek, M. Amorphous Silicon Solar Cells Made with SnO2:F TCO Films Deposited by Atmospheric Pressure CVD. *Mater. Sci. Eng. B* **2009**, 159–160, 6–9.

(22) Müller, J.; Rech, B.; Springer, J.; Vanecek, M. TCO and Light Trapping in Silicon Thin Film Solar Cells," *Sol. Energy*, **2004**, 77 (6), 917–930.

(23) Beyer, W.; Hüpkes, J.; Stiebig, H. Transparent Conducting Oxide Films for Thin Film Silicon Photovoltaics. *Thin Solid Films* **2007**, 516 (2–4), 147–154.

(24) Ohta, H.; Nomura, K.; Hiramatsu, H.; Ueda, K.; Kamiya, T.; Hirano, M.; Hosono, H. Frontier of Transparent Oxide Semiconductors. *Solid-State Electron.* **2003**, 47 (12), 2261–2267.

(25) Hosono, H. Recent Progress in Transparent Oxide Semiconductors: Materials and Device Application. *Thin Solid Films* **2007**, 515 (15), 6000–6014.

(26) Franzen, S. Surface Plasmon Polaritons and Screened Plasma Absorption in Indium Tin Oxide Compared to Silver and Gold. *J. Phys. Chem. C* **2008**, 112 (15), 6027-6032

(27) Kim, J.; Naik, G. V.; Emani, N. K.; Guler, U.; Boltasseva, A. Plasmonic Resonances in Nanostructured Transparent Conducting Oxide Films, *IEEE J. Sel. Top. in Quantum Electron.* **2013**, 19 (3), 4601907.

(28) Honda, S.; Takakura, H.; Hamakawa, Y.; Muhida, R.; Kawamura, T.; Harano, T.; Toyama, T.; Okamoto, H. Carrier Transport in Polycrystalline Silicon Thin Film Solar

Cells Grown on a Highly Textured Structure. *Jpn. J. Appl. Phys*. **2004**, 43 (9R), 5955.

(29) Hegedus S. S.; Kaplan, R. Analysis of Quantum Efficiency and Optical Enhancement in Amorphous Si p–i–n Solar Cells. *Prog. Photovolt. Res. Appl*. **2002**, 10 (4), 257–269.

(30) Wong, A.; Wang, X.; Liu, J. Nano-Needle Structured, Ambipolar High Electrical Conductivity SnO_x ($x \leqslant 1$) Thin Films for Infrared Optoelectronics. *J. Appl. Phys.* **2015**, 117, 103109, 1-7.

(31) Wang, X.; Wong, A.; Malek, S.; Cai, Y.; Liu, J. High-Performance Infrared Light Trapping in Nano-Needle Structured p+ SnO_x ($x \leq 1$)/Thin Film n-Ge Photodiodes on Si. *Opt. Lett.* **2015**, 40 (11), 2603-2606.

(32) Wang, X.; Wong, A.; Yu, X.; Kong, J.; Liu, J. Nanostructured Conductive SnO_x ($x < 2$) for High Efficiency Light Trapping in Thin film and 2D Material Photonic Devices. *Novel Optical Materials and Applications* **2015**, NM4C, 3.

(33) Ferrari, A. C. Raman Spectroscopy of Graphene and Graphite: Disorder, Electron–Phonon Coupling, Doping and Nonadiabatic Effects. *Solid State Commun*. **2007**, 143 (1-2), 47–57.

(34) Wang, L.; Zhao, J.; Sun, Y.-Y.; Zhang, S. B. Characteristics of Raman Spectra for Graphene Oxide from AB Initio Simulations. *J. Chem. Phys*. **2011**, 135 (18), 184503.

(35) Åhlgren, E. H.; Hämäläinen, S. K.; Lehtinen, O.; Liljeroth, P.; Kotakoski, J. Structural manipulation of the graphene/metal interface with Ar+ irradiation, *Phys. Rev. B* **88**, 155419 (2013).

(36) Dlubak, B.; Seneor, P.; Anane, A.; Barraud, C.; Deranlot, C.; Deneuve, D.; Servet, B.; Mattana, R.; Petroff, F.; Fert, A. Are Al_2O_3 and MgO Tunnel Barriers Suitable for Spin Injection in Graphene? *Appl. Phys. Lett.* **2010**, 97, 092502.

(37) Jin, Z.; Su, Y.; Chen, J.; Liu, X.; Wu, D. Study of AlN Dielectric Film on Graphene by Raman Microscopy. *Appl. Phys. Lett.* **2009**, 95, 233110.

(38) Campion, A.; Kambhampati, P. Surface-enhanced Raman Scattering. *Chem. Soc. Rev.* **1998**, 27, 241-250.

(39) Hayt, W. H.; Buck, J. A. Engineering Electromagnetics, Sixth Edition, *McGraw-Hill Series in Electrical and Computer Engineering*, **2000**.

(40) Geurts, J.; Rau, S.; Richter, W.; Schmitte. F. J. SnO Films and Their Oxidation to SnO_2: Raman Scattering, IR Reflectivity and X-ray Diffraction Studies. *Thin Solid Films* **1984**, 121 (3), 217-225.

(41) Olijnyk, H. Pressure Dependence of Raman Phonons of Metallic β -Sn. *Physics Review B* **1992**, 46 (10), 6589-6591.

(42) Adopted from http://ecee.colorado.edu/~ecen4375/s10/secure/L8%20Deposition.pdf.

(43) Takeuchi, K.; Adachi, S. Optical properties of β-Sn films. *J. Appl. Phys.* **2009**, 105 (7), 073520.

(44) Craciun, M. F.; Russo, S.; Yamamoto, M.; Tarucha, S. Tunable Electronic Properties in Graphene. *Nanotoday* **2011**, 6 (1), 42-60.

(45) Brouillet, J.; Papadakis, G. T.; Atwater H. A. Experimental Demonstration of Tunable Graphene-Polaritonic Hyperbolic Metamaterial. *Opt. Express* **2019**, 27, 30225-30232.

(46) Liu, M.; Yin, X.; Ulin-Avila, E.; Geng, B.; Zentgraf, T.; Ju, L.; Wang, F.; Zhang X. A Graphene-based Broadband Optical Modulator. *Nature* **2011**, 474, 64-67.

(47) Reina, A.; Jia, X.; Ho, J.; Nezich, D.; Son, H.; Bulovic, V.; Dresselhaus, M. S.; Kong, J. Large Area Few-Layer Graphene Films on Arbitrary Substrates by Chemical Vapor Deposition. *Nano Lett.* **2009**, 9 (1), 30−35.

(48) Wang, H.; Leong, W. S.; Hu, F.; Ju, L.; Su, C.; Guo, Y.; Li, J.; Li, M.; Hu, A.; Kong, J. Low-Temperature Copper Bonding Strategy with Graphene Interlayer. *ACS Nano* **2018**, 12 (3), 2395−2402.

For Table of Contents Only